Comparison of nonlinear strain path correction models for the FLD characterization

Grégoire Mainguy[1,2*], *Tudor* Balan[1], and *Xavier* Lemoine[2]

[1]Arts et Metiers Institute of Technology, Université de Lorraine, LCFC, F-57070Metz, France
[2]Global R&D ArcelorMittal Maizières, voie Romaine, BP30320, F-57283 Maizières-lès-Metz, France

Abstract. The Forming Limit Diagram (FLD), along with the Forming Limit Curve (FLC) it encompasses, are widely used tools in sheet metal forming to predict the forming behavior of sheet metal. The experimentally determined FLD depend to some extent on the stretching tests used, like the Nakajima or Marciniak tests. Numerous correction models have been proposed over the last 50 years for the effects of the non-linear strain path, curvature, or normal stress. The purpose of this paper is to summarize and compare the mathematical formulations and properties of existing correction models for the non-linear strain path influence on the Nakajima test results. It appears from the analysis that a large number of the available models share identical hypotheses and results, which simplifies and further guides the user's efforts in selecting the adequate correction model.

Keywords: Forming Limit Curve; Strain path; Steel; Correction models

1 Introduction

The foundations of what later became known as Forming Limit Diagrams (FLD) date back to the work of Gensamer in 1946 [1]. He was the first researcher to characterize formability by the local strains only, whatever the particular type of forming process. He plotted the limit strains associated to each stress ratio on a rectangular diagram using the longitudinal and transverse principal strains as abscissa and ordinate which can be considered as the first representation of the Forming Limits Diagram.

Despite Gensamer's innovation, it was not until the 1960s that the concept of formation limit diagrams received widespread attention in the scientific community. Between 1963 and 1968, Keeler and Backofen and then Goodwin revisited and valorized the Forming Limit Diagram concept [2-4]. Their combined work laid the foundation for what is now known as FLD, a standard tool in sheet metal forming analysis.

However, when industrial forming processes are considered, the real strain path of the formed material point is often non-linear unlike for the standardized Forming Limit Curve (FLC) characterization, obtained under a proportional loading condition. According to the experimental studies of Nakajima [5], Müschenborn and Sonne [6], Kleemola et al. [7], Bergström and Ölund [8], Graf and Hosford [9,10] and others [11-13], the strain path has a strong influence on the shape and position the traditional FLC, implying that traditional FLD should only be applied to forming processes with linear strain paths.

In recent years, this topic has attracted renewed attention. Indeed, with the evolution of FLD characterization standards (ISO12004-2 [14], SEP1240 [15], ASTM [16]), it was clearly noticed that the tooling influences the strain paths and that the latter are no longer linear when using a Nakajima punch [17,18].

So, in order to adapt and predict the formability limits of steels for complex strain paths, many new graphical representations as well as strain-path correction methods have been developed. This article aims to review and compare some of them, mathematically and experimentally, and in particular to show the equivalence of the methods presented here.

2 Graphical representation for path-independent forming curves

In order to establish a path independent FLD, several new forms of FLD have been developed [19]; most of them can be divided in two categories: equivalent strain based FLD and stress-based FLD.

2.1 FLD representation using the equivalent strain

Instead of employing the usual representation of the FLD in (ε_2; ε_1) axes, Mesrar [20] proposed in 1998 to plot the equivalent strain (ε_{eq}) at necking as a function of the ratio of the principal strain rates (β):

$$\varepsilon_{eq} = f(\beta) \quad (1)$$

* Corresponding author: gregoire.mainguy@arcelormittal.com

© The Authors, published by EDP Sciences. This is an open access article distributed under the terms of the Creative Commons Attribution License 4.0 (https://creativecommons.org/licenses/by/4.0/).

with:

$$\beta = d\varepsilon_2/d\varepsilon_1 \quad (2)$$

To determine the equivalent strain and strain rate ratio, a yield function must be assumed. The yield criterion of von Mises and the Hill normal anisotropy criteria are often used for this purpose. Mesrar et al [20] also showed the strain path independence of the XFLD, using an MK model.

More recently, the concept of Polar Effective Plastic Strain Diagram (PEPSD) was proposed by Stoughton and Yoon [21]. This representation allows to keep a similar shape with the strain FLD while plotting the equivalent strain (ε_{eq}) versus angle (θ) which is function of strain rate ratio (β):

$$\theta = \tan^{-1}(\beta) \quad (3)$$

The only difference is that PEPSD is plotted in polar coordinates ($\varepsilon_{eq}\sin(\theta)$; $\varepsilon_{eq}\cos(\theta)$) instead of cartesian coordinates. Thus, equivalent strains iso-lines are represented as concentric circles in PEPSD instead of horizontal lines as in [20].

Alternative diagrams have been introduced [22,23] which plot the equivalent strain vs. the stress triaxiality η or vs. the stress ratio α.

With the von Mises yield criterion, and considering the plane stress condition ($\sigma_3 = 0$), the stress ratio and stress triaxiality can be analytically related to the strain ratio as:*

$$\alpha = \frac{1+2\beta}{2+\beta} = \sigma_2/\sigma_1 \quad (4)$$

$$\eta = \frac{1}{\sqrt{3}} \cdot \frac{1+\beta}{\sqrt{1+\beta+\beta^2}} = \sigma_{mean}/\sigma_{eq} \quad (5)$$

Thus, since α and η are univocal functions of the strain ratio β, all these graphical representations would exhibit the same strain-path dependency, if any.

2.2 Stress-Based Forming Limit Curve

Introduced for the first time by the research group of Embury [24,25] and later developed by Arrieux [26] and Stoughton [27], the concept of Stress-based Forming Limit Diagram (σFLD or FLSD) suggests that the formability of sheet metals should be based on stress state rather than strain state. Thereby, the FLSD represents the forming limits with the in-plane principal stress components (σ_2; σ_1).

While the methods based on the equivalent strain require only the recorded strain paths and a chosen yield function, a hardening law is also needed to obtain the FLSD and transform the forming limit strains into forming limit stresses.

Here also, alternative diagrams using stress-based limits have been introduced [19]. The equivalent stress can be plotted as a function of stress ratio α and the resulting diagram can be further transformed in polar coordinates ($\sigma_{eq}\sin(\psi)$; $\sigma_{eq}\cos(\psi)$) with:

$$\psi = \tan^{-1}(\alpha) \quad (6)$$

In 2007, the Extended Stress Forming Limit Diagram (XFLSD) based on equivalent plastic stress versus mean stress was proposed by Simha et al. [28] assuming that the stress states at the onset of necking under plane stress loading are equivalent to those under three-dimensional loading [29,30]. Many stress-based FLDs consider the effect of through thickness stress. Let us remind that during the Nakajima tests, the curvature of the punch linked with significant sheet thicknesses could question the hypothesis of plane stress.

The literature generally reports that all FLSDs, based on phenomenological plasticity models such as Hill (1948) and Hosford (1979), were nearly path independent. The main reason is the decreasing slope of the hardening curve: in the plastic domain, even a large increase in equivalent strain leads to only a small increase in equivalent stress. However, those stress-based diagrams have two major drawbacks: obtaining experimental data for the stress space compared to the strain space is difficult [31].

As shown in Figure 1, the diagrams that use either the triaxiality or the mean stress σ_{mean} require knowing the value of σ_3, unless the plane stress condition ($\sigma_3 = 0$) is assumed. Moreover, Figure 1 shows that the use of FLD, equivalent strain FLD and stress based FLD gives the same information as long as the functions used to move from one representation to another are bijections. But this is not the case with the calculation of equivalent strain as well as the equivalent stress if kinematic or distortional hardening are used. Thus, if isotropic hardening is used, equivalent strain FLD and stress based FLD must contain the same information.

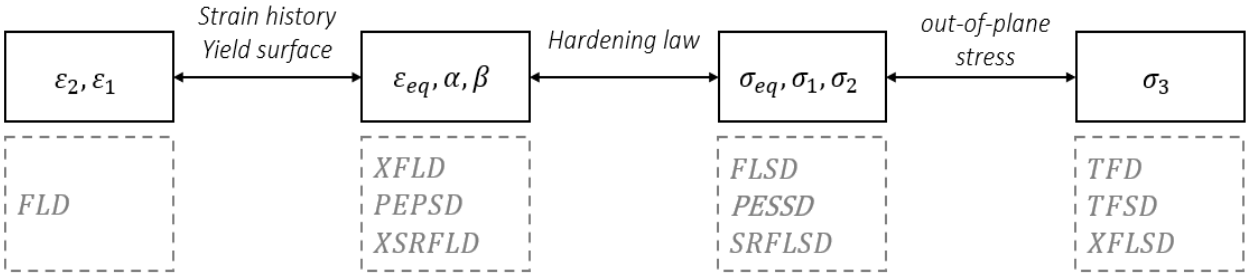

Fig. 1. Various FLD representations, the represented quantities and the plasticity equations required for their application

3 Correction of strain-path non-linearity after FLD characterization

In parallel with the appearance of some independent strain path graphical representations, mathematical models have been proposed to correct the nonlinearity of strain paths after the FLD characterization, in order to retrieve the material's "linear" FLD. The first models were applied to bilinear strain path, composed of a linear pre-strain, an unload and a standard FLD characterization. Thus, in the diagrams where the equivalent strain or stress is plotted with respect to α, β or η, the change between the two linear strain paths is represented by a horizontal offset.

Grumbach and Sanz [32], Müschenborn and Sonne [6], and more recently Aretz [33], have used the equivalent strain to reduce a bilinear path to an equivalent fictitious linear path, based on empirical interpretations. Indeed, the numerous tests made by Grumbach and Sanz, Müschenborn and Sonne and others [9-11] suggest that the position of this particular fictitious FLD point with direct path would be representative of the formability of the bilinear path.

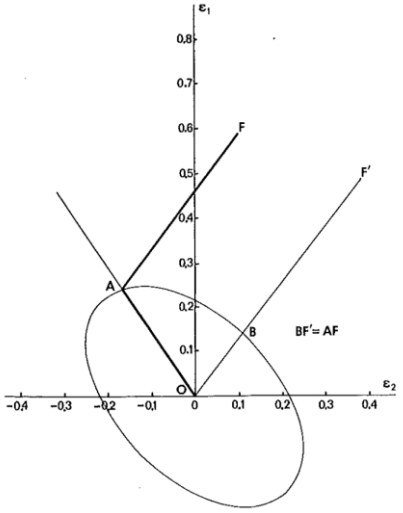

Fig. 2. Construction of the Grumbach-Sanz method [32]

Their idea is to use the ellipses of iso-values of the equivalent strain and propose the construction shown in Figure 2. According to their hypothesis, the formability limit at point F for the bilinear path OAF, corresponds to the one at point F' for the linear path OBF', since the equivalent strain is identical in A and B. Thus, the formability limit would correspond to a critical value of equivalent strain characteristic of the last strain path experienced by the material.

Let us note respectively $\|OA\|$ the von Mises equivalent strain between points OA, and $\overline{OA}_{FLC}$ the length of the segment $\overline{OA}$ in the FLD. One can then note:

$$\|OA\| = \int_O^A \dot{\varepsilon_{eq}}\, dt = \int_O^A \frac{2}{\sqrt{3}}\sqrt{1+\beta+\beta^2}\,\dot{\varepsilon_1} dt \quad (7)$$

and for linear strain paths:

$$\|OA\| = \frac{2}{\sqrt{3}}\sqrt{1+\beta_{[OA]}+\beta_{[OA]}{}^2}\,(\varepsilon_1^A - \varepsilon_1^O) \quad (8)$$

The geometric method in [32], as well as the methods in [6] and [33], can be written as:

$$\|OA\| + \|AF\| = \|OF'\| \quad (9)$$

Aretz [33] developed the Equation (9) in order to obtain bilinear strain path FLC from direct FLC and vice versa. He applies this correction to the Nakazima tests by assuming that pre-straining occurred under balanced biaxial tension, and that the minor strain value of the pre-strains equals the minor strain of the lowest point of the FLD. This is, of course, only an approximation. As illustrated for example by Gutiérrez et al. [17], the strain ratio β changes continuously during a Nakajima test.

In 2006, Leppin [34] extended this empirical observation to a continuous stain path. He assumed that as long as there is the same strain ratio at the end (β_{end}) of the strain path, the FLC points will have the same equivalent strain. In other words, for each ratio β, there would be only one unique limit whatever the deformation path.

Then, Min et al. [35] used the same hypothesis and considered continuous strain paths recorded by Digital Image Correlation (DIC). They calculated the corresponding equivalent strains as a sum of n small linear strain paths. The points composing the real strain path are noted O_i and O_n is the corrected point for a linear strain path:

$$\|OO_n\| = \sum_{i=0}^{n-1}\|O_iO_{i+1}\| = \frac{2}{\sqrt{3}}\sqrt{1+\beta_{end}+\beta_{end}{}^2}\,\varepsilon_1^{O_n} \quad (10)$$

They further combined the resulting strain path correction with additional corrections for curvatures and normal pressures and obtained convincing results for DP sheet steels.

The correction methods presented in this section [6, 32, 33] are therefore all based on the same assumption: the equivalent strain-based FLD is supposed strain paths independent. Thus, when plotting nonlinear FLCs in an equivalent strain-based space, the corrected points must be superimposed on the uncorrected points. Moreover, according to the conclusions of Section 2, the same observation should be made for stress-based FLD if isotropic hardening is used, as for diagrams using triaxiality or mean stress σ_{mean} if plane stress conditions are respected.

4 Application to bilinear FLCs of sheet steel

In order to illustrate the conclusion of Section 3, direct and bilinear FLDs of a 0.8 mm thick mild steel sheet were used to explore the usefulness of the above mentioned FLD representations and correction methods. Although different materials may exhibit distinct responses to nonlinear deformation paths, the role of this section is to visualize the impact of the choice of graphical representation on the FLC and to show that strain path correction is no longer necessary when using non-traditional FLD. The material's mechanical characteristics are shown in Table 1.

Table 1. CR4 sheet mild steel mechanical characteristics

Steel	*t*	Direction	$Rp_{0.2}$	*Rm*	*A*	*Ag*	*r*	*n*
CR4	0.8mm	90°	171 MPa	319 MPa	38	21.2	2.12	0.21

The FLD points in the extension area were obtained through hydraulic bulge tests and the points in the shrink area were obtained through tensile tests. Hydraulic bulge tests assess the formability of sheet metal by applying fluid pressure through various elliptical die geometries, covering a range from plane tension (excluded) to equibiaxial stretching. The ellipsis' large axis equal to 150mm and the small axis between 50 and 150mm. As with tensile testing, the strain paths of bulge tests can be considered linear, which is not the case with Nakajima tests [36]. The strain analysis was performed with GOM's Aramis and in accordance with the analysis proposed in the ISO12004-2 standard. In the following figures, the direct FLD is designated by circular symbols. For the bilinear FLD, all the samples were pre-strained up to the pre-strain point of coordinates (-0.088; 0.12), denoted with a diamond. The square symbols show the experimental points of the FLC subsequent to this pre-strain. Finally, the triangles represent the correction of the bilinear FLC with the "equivalent-strain-method" presented in Section 3. The symbols are resume in Figure 3:

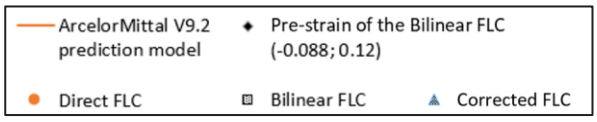

Fig. 3. Legends for Figures 4 to 13

In addition to these experiments, the ArcelorMittal V9.2 model [37] was used to predict the direct FLC of the material. Based on the theories of plastic flow, plastic instability and damage, the model predicts the direct FLC based on the input values of R_m, A_g, *r,* and *t*.

As Figure 4 shows, in a standard strain space, the bilinear and the linear FLCs are very different. In turn, the strain path correction brings the bilinear FLC close to the linear one, especially considering the inherent experimental error range. The von Mises equivalent strain was used for the strain-path correction, cf. eq. (7).

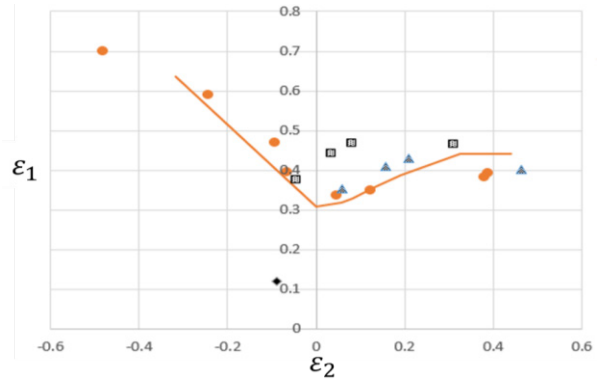

Fig. 4. Standard representation of the FLD for linear, bilinear, and corrected bilinear experimental points.

Figures 5 to 7 show alternative FLD representations based on the equivalent strain. As expected, the application of the strain path correction method does not change the coordinates of the points of the bilinear FLC, confirming the theoretical path-independence of these representations.

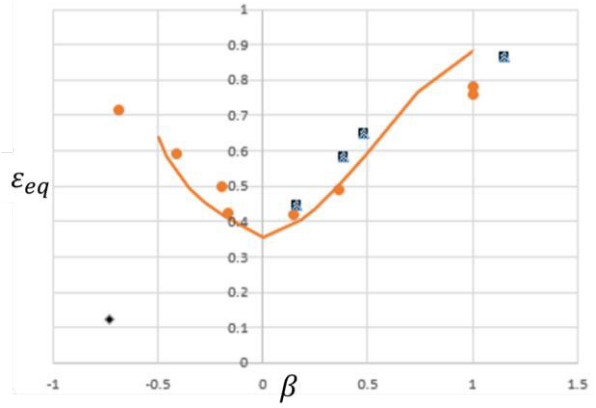

Fig. 5. (ε_{eq}, β) representation for linear, bilinear, and corrected bilinear experimental points.

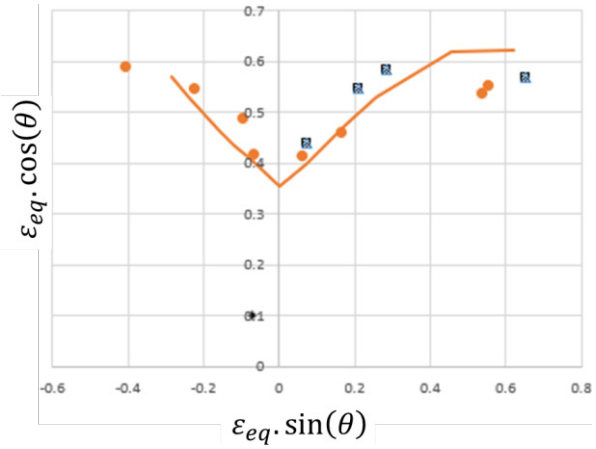

Fig. 6. PEPS representation for linear, bilinear, and corrected bilinear experimental points.

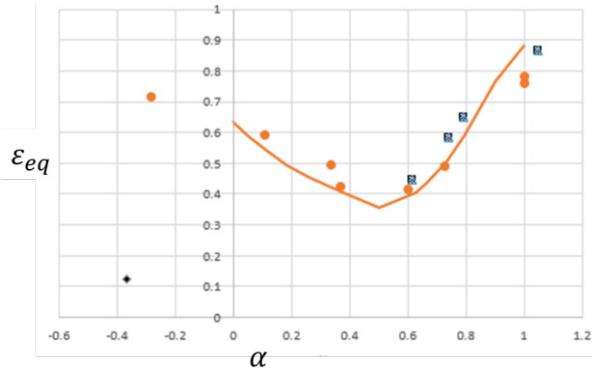

Fig. 7. (ε_{eq}, α) representation for linear, bilinear, and corrected bilinear experimental points

In order to plot the stress-based FLDs, we chose the combined Swift-Voce hardening law, equation (11), whose coefficients, fitted from tensile tests, are listed in Table 2:

$$\sigma_{eq} = K(1-\alpha)\left(\varepsilon_0 + \varepsilon_{eq}\right)^n + \alpha[\sigma_0 + R_{sat}(1 - e^{-C_r.\varepsilon_{eq}})] \quad (11)$$

Table 2. Swift-Voce coefficients

ε_0	K	n	σ_0	R_{sat}	Cr	α
0.006	592MPa	0.254	173 MPa	230 MPa	12.9	0.4662

The various stress-based FLDs in Figures 7 to 9 show that the different curves overlap very well. It is noteworthy that these three figures do not contain more information than Figures 4 to 7 since the Swift-Voce hardening law is a bijection function from [0;+∞[to [0;+∞[. Although the gap between points appears smaller than for equivalent strain-based representations, stress-based FLCs are as independent of the strain path as the equivalent-strain-based ones. The saturation of the hardening law converts strain discrepancies into apparently smaller stress discrepancies between different points, which however convey the same information on path-independence.

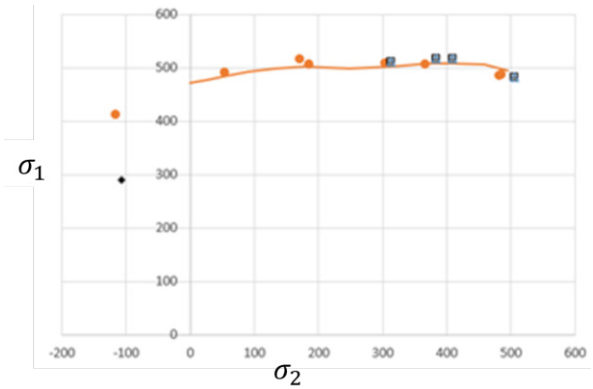

Fig. 8. FLSD representation for linear, bilinear, and corrected bilinear experimental points.

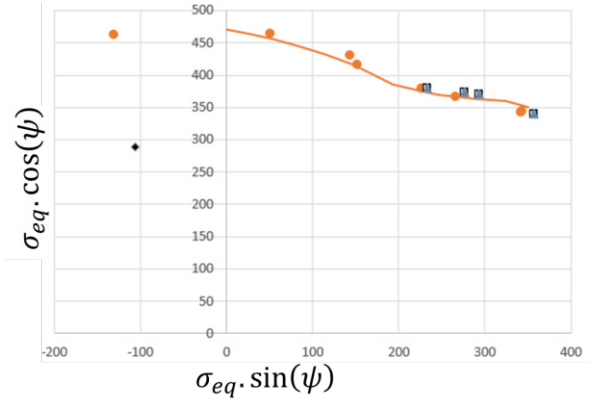

Fig. 9. PESSD representation for linear, bilinear, and corrected bilinear experimental points.

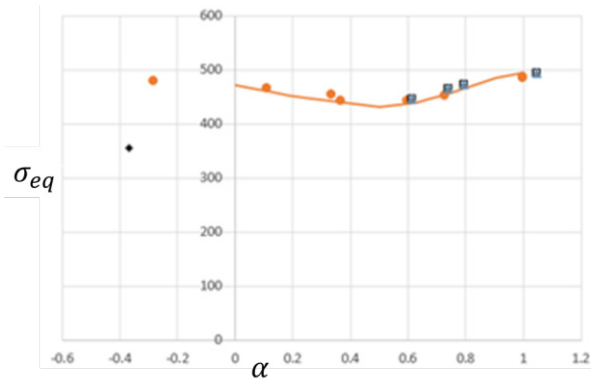

Fig. 10. (σ_{eq}, α) representation for linear, bilinear, and corrected bilinear experimental points.

The final series of FLD representations makes use of the stress triaxiality or the mean stress. As shown in Figures 10 to 12, they are similar to the above representations. This is because a state of plane stresses has been considered ($\sigma_3 = 0$).

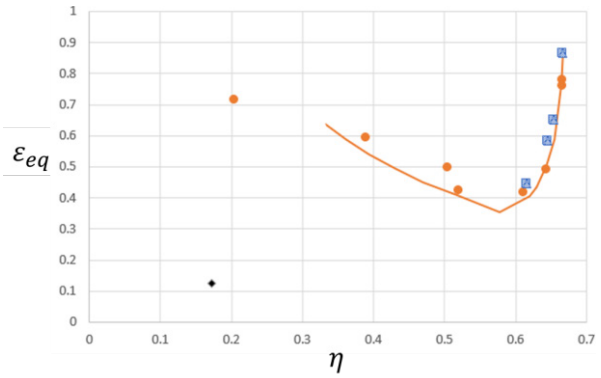

Fig. 11. (ε_{eq}, η) representation for linear, bilinear, and corrected bilinear experimental points.

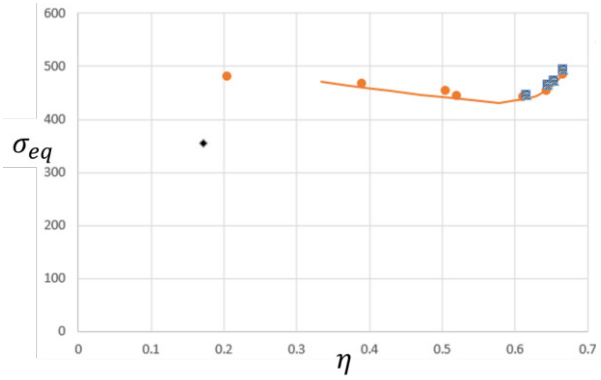

Fig. 12. (σ_{eq}, η) representation for linear, bilinear, and corrected bilinear experimental points.

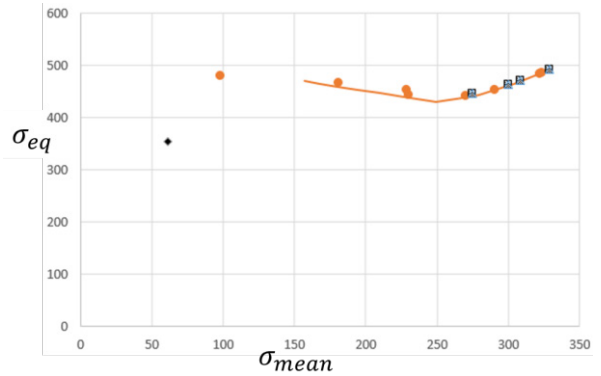

Fig. 13. XFLSD representation for linear, bilinear, and corrected bilinear experimental points.

These experimental results then make it possible to provide several conclusions and warnings. The first is that, as long as isotropic hardening is used and plane stress conditions are respected, the choice of graphical representation is of little importance. The second is that while the path independence of stress-based FLDs (Figures 8-10,12,13) may seem visually more accurate than that of the equivalent-strain-based ones, they contain exactly the same information but after a nonlinear change of variables that shrinks the discrepancies at larger strains. Finally, these figures given that stress-based representations require additional assumptions about the material model, the strain-based representations are more appealing without

any loss of accuracy. This will allow a better understanding of the dispersion of the experimental points.

5 Conclusions

In this paper, an investigation of non-linear strain-path correction and graphical representations of was carried out. Several conclusions could be drawn:

Most of the available correction methods are based on the same assumption of the conservation of the equivalent strain. And all the discussed correction methods are equivalent to each other.

Strain path-independent graphical representations of FLD can be separated into three groups: equivalent-strain FLD/ Stress-based FLD/ through-thickness-stress FLD.

The use of stress based FLD gives the same information as equivalent strain FLD if the hardening law used is a bijection, meaning that it does not include kinematic or distortional hardening.

The use of equivalent-strain FLD and stress-based FLD gives the same information as through-thickness-stress FLD if a state of plane stresses is considered.

Further research must be performed to provide a clearer physical basis to the assumption of equivalent strain correction. Indeed, several authors have shown that the assumption is no longer valid if the pre-strain is significant [38].

References

1. M. Gensamer, Trans. Am. Math. Soc. **36**, 30 (1946)
2. S. P. Keeler, *Plastic Instability and fracture in sheets stretched over rigid punches*, Doctoral dissertation, Massachusetts Institute of Technology (1961)
3. S. P. Keeler, SAE Tech. Pap. **650535** (1965)
4. G.M. Goodwin, SAE trans, 380 (1968)
5. K. Nakazima, T. Kikuma, K. Hasuka, Yamata Tech. Rep. **264**, 8517 (1968)
6. W. Müschenborn, H.M. Sonne, Arch. Eisenhüttenw. **46**, 97 (1975)
7. H.J. Kleemola, M.T. Pelkkikangas, Sheet Met. Ind. **63**, 591 (1977)
8. Y. Bergström, S. Ölund, Mater. Sci. Eng. C. **56**, 47 (1982)
9. A. Graf, W.F. Hosford, Metall. Trans. **24**, 2497 (1993)
10. A. Graf, W.F. Hosford, Int. J. Mech. Sci. **36**, 897 (1994)
11. J.V. Laukonis, A.K. Ghosh, Metall. Trans. **9**, 1849 (1978)
12. A.K. Ghosh, W.A. Backofen, Metall. Trans. **4**, 1113 (1973)
13. T. Kobayashi, *Effect of strain ratios on the deforming limit of steel sheet and its application to the actual press forming,* in Proceedings of the International Deep Drawing Research Group. IDDRG Amsterdam (1972)
14. ISO, *Metallic materials – guidelines for the determination of forming-limit diagrams* International Standard ISO 12004-2 (2019)
15. SEP 1240, *Testing and Documentation Guideline for the Experimental Determination of Mechanical Properties of Steel Sheets for CAE-Calculations* (2006)
16. ASTM E2218-15, ASTM Book of Standards, 1-15 (2015)
17. D. Gutierrez, *Strain path effects on the formability of AHSS evaluated by stretching test,* in Proceedings of the International Deep Drawing Research Group. IDDRG (2009)
18. M. Abspoel, E.H. Atzema, *Inherent influence of strain path in Nakazima FLD testing,* in Proceedings of International Deep Drawing Research Group. IDDRG, Mumbai, India (2011)
19. S.K. Paul, J. Manuf. Process, **20**, 291 (2015)
20. R. Mesrar, S. Fromentin, R. Makkouk, M. Martiny, G. Ferron, Int. J. of plasticity, **14**, 391 (1998)
21. T.B. Stoughton, J.W. Yoon, Int. J. Solids Struct. **49**, 3616 (2012)
22. S.K. Paul, J. Strain. Anal. Eng. Des. **48**, 177 (2013)
23. K. Yoshida, T. Kuwabara, M. Kuroda, Int. J. Plast, **23**, 361 (2007)
24. G. Glover, G.L. Duncan, J.D. Embury, Met. Tech. **4,** 153 (1977)
25. D.J. Lloyd, H. Sang, J.D. Embury, Mater. Sci. Eng. C **36**, 35 (1978)
26. R. Arrieux, C. Bedrin, M. Boivin, *Determination of an intrinsec forming limit stress diagram for isotropic sheets*, In Proceedings of the 12th International Deep Drawing Research Group. IDDRG (1982)
27. T.B. Stoughton, Int. J. Mech. Sci. **42**, 1 (1999)
28. C.H.M. Simha, J. Gholipour, A. Bardelcik, M.J. Worswick, ASME. J. Eng. Mater. Technol. **129,** 36 (2007)
29. D. Banabic, Int. J. Mater. Form. **13,** 749 (2020)
30. H. Zhu, Z. He, Y. Lin, K. Zheng, X. Fan, S. Yuan Int. J. Mech. Sci. **172,** 105392 (2020)
31. T.N. Zaman*, Effects of strain path changes on damage evolution and sheet metal formability*, Doctoral dissertation, McMaster University, Hamilton, Ontario (2008)
32. M. Grumbach, G. Sanz, Mem. Sci. Rev. Met. **11**, 659 (1974)
33. H. Aretz, Mater. Res. Proc. **41,** 948 (2024)
34. C. Leppin, *Application of a method to correct the effect of non-proportional strain paths on Nakajima test based forming limit curves*. Proceedings of 7th Numisheet (2008)
35. J. Min, TB. Stoughton, JE. Carsley, J. Lin, Int. J. Mech. Sci, **117**, 115 (2016)
36. J. Noder, C. Butcher, Int. J. Mech. Sci, **163**, 105138 (2019)
37. F. Cayssials, X. Lemoine, *Predictive model of FLD (Arcelor model) upgraded to UHSS Steels,* in Proceedings of the International Deep Drawing Research Group. IDDRG, Besançon, France (2005)
38. Y.P. Korkolis, S. Kyriakides, Int. J. Plast. **25,** 2059 (2009)